Cap-binding protein 4EHP effects translation silencing by microRNAs

The cap-binding protein 4EHP effects translation silencing by microRNAs

Clément Chapat[1,a,b], Seyed Mehdi Jafarnejad[1,a,b], Edna Matta-Camacho[a,b], Geoffrey G. Hesketh[c], Idit A. Gelbart[d], Jan Attig[e], Christos G. Gkogkas[f], Tommy Alain[g], Noam Stern-Ginossar[d], Marc R. Fabian[h], Anne-Claude Gingras[c,i], Thomas F. Duchaine[a,b,2] and Nahum Sonenberg [a,b,2]

[1] These authors contributed equally to this manuscript

[a] Goodman Cancer Research Center, McGill University, Montreal, QC H3A 1A3, Canada

[b] Department of Biochemistry, McGill University, Montreal, QC H3A 1A3, Canada

[c] Centre for Systems Biology, Lunenfeld-Tanenbaum Research Institute, Sinai Health System, Toronto, Ontario, Canada

[d] The Department of Molecular Genetics, Weizmann Institute of Science, Rehovot, Israel

[e] The Francis Crick Institute, London, NW1 1AT, United Kingdom

[f] Patrick Wild Centre, Centre for Integrative Physiology, University of Edinburgh, Edinburgh, EH8 9XD, UK

[g] Children's Hospital of Eastern Ontario Research Institute, Department of Biochemistry, Microbiology and Immunology, University of Ottawa, Ottawa, Ontario, Canada

[h]Lady Davis Institute for Medical Research, McGill University, Montreal, QC H3A 1A3, Canada

[i] Department of Molecular Genetics, University of Toronto, Toronto, Ontario, Canada

[2] Correspondence: nahum.sonenberg@mcgill.ca, thomas.duchaine@mcgill.ca

Abstract

MicroRNAs (miRNAs) play critical roles in a broad variety of biological processes by inhibiting translation initiation and by destabilizing target mRNAs. The CCR4-NOT complex effects miRNA-mediated silencing at least in part through interactions with 4E-T (eIF4E-Transporter) protein, but the precise mechanism is unknown. Here we show that the cap-binding eIF4E-Homologous Protein 4EHP is an integral component of the miRNA-mediated silencing machinery. We demonstrate that the cap-binding activity of 4EHP contributes to the translational silencing by miRNAs through the CCR4-NOT complex. Our results suggest that 4EHP competes over eIF4E for binding to 4E-T, and this interaction increases the affinity of 4EHP for the cap. We propose a model wherein the 4E-T/4EHP interaction triggers the assembly of a closed loop mRNA conformation that blocks translational initiation of miRNA targets.

Keywords: microRNA, miRNA, mRNA translation, eIF4E2, 4EHP, 4E-T, CCR4-NOT, eIF4E, eIF4F

Statement of significance

miRNAs are important components of gene regulatory networks and affect virtually all aspects of cell biology by controlling the stability and translation efficiency of their target mRNAs. Here we identified the mRNA cap-binding eIF4E-related protein, 4EHP as an effector of miRNA-mediated translation repression. Through screening for protein interactions in cells via the BioID method, we identified 4EHP as a component of the CCR4-NOT/DDX6/4E-T axis. Direct interaction between 4E-T and 4EHP increases the latter's cap-binding affinity, suggesting that this interaction potentiates its competition with the eIF4F complex for binding to the mRNA 5´cap. Our findings suggest that 4EHP facilitates the formation of a closed-loop structure between the 3´ UTR of the mRNA and its 5´cap, which causes repression of mRNA translation.

\body

INTRODUCTION

MicroRNAs (miRNAs) are short ~22-nucleotide noncoding RNAs that affect gene expression in most eukaryotes. miRNAs mediate post-transcriptional silencing by guiding the miRNA-induced silencing complex (miRISC), an assembly of Argonautes and GW182/TNRC6 proteins, to target mRNAs. Target recognition initiates a succession of events: mRNA translational repression, deadenylation and mRNA decay (1). miRNAs impair the function of eIF4F on mRNAs, a three-subunit complex composed of eIF4E, the m^7GTP (cap)-interacting factor, eIF4G, a scaffolding protein, and eIF4A, a DEAD-box RNA helicase (2-5). The silencing activity of miRISC is mediated by the CCR4–NOT deadenylase complex through the scaffolding subunit, CNOT1 (6-8). CNOT1 recruits the DDX6 and 4E-T (eIF4E-Transporter) proteins and their interaction is important for miRNA-mediated silencing (9-16). 4E-T is a conserved eIF4E-binding protein, which directly binds to the dorsal surface of eIF4E through its canonical eIF4E-binding YX_4LL (Y^{30}TKEELL) motif, and impairs the eIF4E/eIF4G interaction and translation initiation (17). 4E-T also facilitates the decay of CCR4-NOT targeted mRNAs by linking the 3'-terminal mRNA decay machinery to the cap via its interaction with eIF4E (13).

In mammals, eIF4E is the best-studied member of a family of proteins composed of eIF4E (eIF4E1), 4EHP (4E-Homologous Protein; eIF4E2) and eIF4E3. 4EHP and eIF4E3 share respectively 28% and 25% sequence identity with eIF4E (18, 19). 4EHP is a ubiquitously expressed protein, and it is 5-10 times less abundant than eIF4E in a number

of mammalian cell lines (18-20). Like eIF4E, 4EHP binds to 4E-T, but in contrast, it does not associate with eIF4G (18, 21). 4EHP has a 30-100-fold weaker affinity for the cap than eIF4E due to a two amino acid substitution in its cap-binding pocket (22). However, post-translational modifications can improve 4EHP affinity for the cap (23, 24).

4EHP has primarily been studied as a translation repressor. In the *Drosophila* embryo, 4EHP associates with the RNA binding protein Bicoid to repress *caudal* mRNA translation (25). Similarly, 4EHP also represses the *hunchback* mRNA via its interaction with the nanos repressive element (NRE) complex, which consists of nanos, pumilio, and "brain tumor" proteins (26). A similar mechanism functions in mouse, where 4EHP binds the Prep1 RNA-binding protein and inhibits *Hoxb4* mRNA translation (27). Moreover, 4EHP forms a translational repressor complex with GIGYF2 (Grb10-interacting GYF protein 2), which acts as a cofactor in translational repression and mRNA decay of tristetraprolin-targeted mRNAs (28, 29).

In this study, we demonstrate that 4EHP interacts with the mRNA silencing machinery, and engenders miRNA-mediated translational repression. Our data support a model wherein 4EHP interactions with miRISC/CCR4-NOT lead to the translational repression of miRNA targets.

RESULTS

4EHP is a component of the miRISC effector machinery.

The specificity of eIF4E and 4EHP for their mRNA targets and their affinities for the cap are defined by binding partners (2, 28, 30). Thus, we utilized the BioID assay (31) to identify the eIF4E and 4EHP interacting proteins. We created stable cell lines expressing 4EHP or eIF4E fused in-frame with an abortive biotin ligase BirA* (R118G) (Fig. S1A and B). 4EHP and eIF4E proteins were thus used as baits to biotinylate and capture interactors and proteins in close proximity. Biotinylated proteins were isolated using streptavidin-affinity purification under denaturing conditions and analyzed by mass spectrometry (MS). Each bait protein was fused at its N- or C-terminus to BirA* and two independent replicates for each construct were analyzed (4 in total for each bait protein), alongside negative controls. The MS data were processed with the SAINT (Significance Analysis of INTeractome) computational tool (32) using several controls for statistical analysis to assign confidence scores to interaction pairs (Dataset S1; see Materials and Methods). Data were highly consistent across replicates (mean correlation coefficient $R^2 = 0.89$ and 0.94, for 4EHP and eIF4E, respectively; Fig. S1C and D). BioID identified 30 high-confidence targets for 4EHP and 8 for eIF4E (FDR $\leq$ 1%; Fig. 1A and Dataset S1). The list of proteins identified for 4EHP is consistent with previous reports showing that 4EHP interacts with GIGYF1, GIGYF2, ZNF598, and 4E-T proteins (28). Known interactions with eIF4E, such as 4E-BP1 (EIF4EBP1), EIF4G1 and eIFG3, were also detected (33).

Gene ontology analysis showed that "translation" was the biological process with the most significant representation among 4EHP interactions (Fig. 1B and Dataset S2). In contrast with eIF4E, BioID with 4EHP identified several known miRNA co-factors including DDX6, CNOT1, PATL-1 and TNRC6A/B, the scaffolding proteins of miRISC (1). To confirm that 4EHP physically interacts with these proteins, we carried out co-immunoprecipitation (IP) experiments. Due to the poor quality of the commercially available anti-4EHP antibodies for IP assay, lysates prepared from human embryonic kidney (HEK) 293T cells transfected with a vector expressing 3xFlag-4EHP, or an empty vector, were immunoprecipitated with anti-Flag antibody followed by western blotting. FLAG-tagged 4EHP co-precipitated 4E-T and the CNOT1 subunit of the CCR4-NOT complex (Fig. 1C). Likewise, endogenous 4EHP co-precipitated with endogenous DDX6, as well as HA-tagged PATL-1, a physical partner of both CCR4-NOT, DDX6 and 4E-T (12, 34, 35) (Fig. 1D and E). Taken together, these data demonstrate that 4EHP physically associates with several key proteins involved in miRISC/CCR4-NOT-mediated gene silencing.

4EHP effects miRNA-dependent translational repression.

The association of 4EHP with components of miRISC and its effector machinery (CCR4-NOT, 4E-T, DDX6) raised the possibility that 4EHP plays a role in miRNA-mediated silencing. To investigate this, we used a luciferase construct (Fig. 2A) fused to the wild-type (WT) 3′ UTR of the *Hmga2* mRNA (an endogenous target of the let-7 miRNA), or a modified version with point mutations disrupting all seven target sites (36). Reporter constructs were transfected into mouse embryonic fibroblasts (MEFs) from wild-type

(WT) or 4EHP-knockout (KO) mice (Fig. S2A) (28). The reporter containing the wild-type 3′ UTR of *Hmga2* was repressed 4.4 fold in WT MEFs as compared to the mutated, control reporter (Fig. 2A and S2B). This repression was significantly less (1.6-fold) in 4EHP-KO cells, demonstrating that 4EHP is required for the efficient silencing of the *Hmga2* 3´ UTR reporter by the let-7 miRNA. We also examined the impact of 4EHP depletion on silencing of two additional miRNA reporters, in the U251 human glioblastoma cell line and in the human cervical adenocarcinoma HeLa cell line. A luciferase construct containing a portion of the *E2f* 3′ UTR, which is repressed by the miR-17/20a paralogs (37), was significantly de-repressed upon knock-down of 4EHP in U251 cells ((Fig. 2B and S2C). Similarly, depletion of 4EHP (si4EHP) in HeLa cells significantly de-repressed a luciferase reporter harboring three miR-19a-binding sites, in comparison with cells treated with a control siRNA (siCTR) (Fig. S2D and E). De-repression was not due to the differential expression of the miRNAs in 4EHP-depleted cells (Fig. S2F). Altogether, our data indicate that 4EHP contributes to miRNA-mediated silencing by several miRNAs, and in various mammalian cell lines.

CNOT1, the scaffolding subunit of the CCR4-NOT complex, is an established player in miRNA-mediated silencing (6-8). We therefore sought to examine the interaction between 4EHP and CNOT1. To this end, we transfected HEK293T cells with plasmids encoding 3xFlag-4EHP and V5-tagged full-length or truncated variants of CNOT1 (Fig. 2C), and examined their interaction by co-IP. 4EHP co-precipitated with either the full-length CNOT1, or the middle domain (M) of CNOT1 (Fig. 2D). Importantly, the middle domain also interacts with 4E-T via DDX6 (9, 10, 14-16). To investigate if 4EHP plays a role in translation repression by the CCR4-NOT complex, we used the λN-BoxB

tethering approach (38). We employed a RL reporter containing five BoxB hairpins in its 3′ UTR. The 3´-end of the reporter contains a self-cleaving hammerhead ribozyme (HhR) to generate an internalized poly(A) stretch of 114 nt, followed by 40 nt to prevent deadenylation and subsequent degradation (39). The reporter was co-transfected into HEK293T cells along with a plasmid encoding a fusion of CNOT1 to a λN peptide, which binds to BoxB elements. Silencing through CNOT1 was examined by comparing the luciferase activity in cells wherein 4EHP was stably depleted via shRNA (sh4EHP) with non-depleted control cells (shCTR). CNOT1 tethering to the BoxB reporter in shCTR cells resulted in a 3.7-fold repression of RL activity, while depletion of 4EHP resulted in significant de-repression of the reporter (1.8-fold; Fig. 2E and S2G). Similarly, siRNA knockdown of 4E-T partially relieved the repression exerted by tethered CNOT1 (1.8-fold vs 2.9-fold repression in siCTR) (Fig. S2H and I). We also examined the role of 4EHP on the repressive activity of the C-terminal silencing domain of human GW182/TNRC6C (GW182(SD); AA 1382–1690), which functions through CNOT1 recruitment (6-8). Consistent with the effects on the miRNA reporters and with the CNOT1 tethering experiment, 4EHP-depletion impinged on the repression exerted by tethered GW182(SD) (1.8-fold de-repression) (Fig. 2E and S2G).

We next examined the importance of the cap-binding activity of 4EHP for miRNA-mediated silencing. We performed a complementation assay using tethered λN-CNOT1 in the presence of WT 4EHP or the $4EHP^{W124A}$ mutant, which is incapable of binding to the cap (19). Transient transfection of shRNA-resistant 3xFlag-4EHP in 4EHP-knockdown cells restored λN-CNOT1-mediated translation repression (Fig. 2F and S2J),

while transfection with 4EHP^{W124A} did not. These results demonstrate that cap binding by 4EHP is required for translation repression effected through CCR4-NOT.

4EHP and eIF4E compete for binding to 4E-T.

4E-T is enriched among 4EHP BioID targets (Fig. 1A), but 4E-T also interacts with eIF4E, and both eIF4E and 4EHP bind the same eIF4E-binding motif of 4E-T (Y^{30}TKEELL) (21). We compared the effects of mutations in this motif on the interactions of 4E-T with 4EHP and eIF4E. We co-transfected HEK293T cells with constructs encoding 3xFlag-4EHP and either WT HA-tagged 4E-T, or 4E-T bearing point mutations in the YTKEELL motif (Y^{30}A and 4A; YTKEELL→AAKEEAA) and tested their interactions by IP. 4E-T co-immunoprecipitated with 4EHP and eIF4E, but both interactions were lost with either mutants of the YTKEELL motif (Fig. 3A). It is noteworthy that wild-type HA-4E-T immunoprecipitated a greater portion of 3xFlag-4EHP, relative to the amount of input, compared with endogenous eIF4E. We thus hypothesized that 4E-T may bind better to 4EHP than to eIF4E (Fig. 3A). To further study this difference, we performed an IP assay in transfected HEK293T cells, which co-expressed constant amounts of HA-4E-T, and incremental amounts of Flag-4EHP (Fig. 3B). While the interaction between HA-4E-T and endogenous eIF4E could be detected in the absence of exogenous 4EHP, overexpression of 4EHP prevented 4E-T binding to eIF4E (Fig. 3B). To further examine these interactions, we prepared recombinant 4EHP, eIF4E and 4E-T proteins and performed *in vitro* binding assays. We compared the 4E-T/4EHP and 4E-T/eIF4E interactions *in vitro* by using constant amounts of HA-4E-T and increasing concentrations of His-4EHP or His-eIF4E (Fig. S3A and B). In such

conditions, 4EHP was 20-30 times more potent than eIF4E for binding to 4E-T (Fig. 3C; Fig. S3C). To corroborate the preference of 4E-T for 4EHP over eIF4E, we performed an *in vitro* displacement assay using pre-associated HA-4E-T/eIF4E immobilized on anti-HA agarose beads. An excess amount of eIF4E was incubated with the 4E-T-bound beads to saturate the binding sites on 4E-T. Preassembled eIF4E/4E-T complexes were next incubated with increasing amounts of recombinant 4EHP. In such conditions, addition of 1.8 µM of 4EHP displaced more than 60% of eIF4E bound to 4E-T (Fig. 3D). Altogether these results suggest that 4EHP has a competitive advantage over eIF4E for binding to 4E-T.

4E-T interaction increases the affinity of 4EHP to m^7GTP cap.

Protein interaction and post-translational modifications can significantly modulate the affinity of eIF4E and 4EHP for the cap (23, 24, 40). In addition to the canonical YTKEELL motif, both 4EHP and eIF4E interact with a secondary non-canonical sequence of 4E-T. However, the contribution of the non-canonical motif appears more important for interaction with 4EHP (21). We thus hypothesized that the extended interaction surface of 4E-T and its greater affinity for 4EHP (Fig. 3) may influence the ability of 4EHP to bind the m^7GTP cap. To test this, we performed an Isothermal Titration Calorimetry (ITC) assay to examine how interaction with 4E-T polypeptides impacted 4EHP affinity for the cap. We used three different 4E-T peptides: one encoding the canonical YTKEELL motif alone (4E-T^{28-37}; Fig. S4A), the same sequence in combination with the non-canonical motif (4E-T^{28-71}), and another, which covers the entire N-terminal extremity (4E-T^{1-265}, Fig. S4A). The 4E-T peptides were pre-incubated

with recombinant 4EHP protein and titrated with m^7GTP. Using this assay, the affinity of 4EHP for m^7GTP was $8.0 \pm 0.56x10^{-6}$ M in the absence of 4E-T peptides (Table 1 and Fig. S4B). Adding the 4E-T^{28-37} peptide did not significant change this affinity. However, the affinity of 4EHP for the m^7GTP cap was 4-fold greater in the presence of the N-terminus of 4E-T (K_D of $5.9 \pm 0.7x10^{-6}$ M and $1.8 \pm 0.4x10^{-6}$ M for 4E-T^{28-71} and 4E-T^{1-265}, respectively; Table 1 and Fig. S4B-E). In comparison, the affinity of eIF4E for the m^7GTP cap (K_D $8.8 \pm 11x10^{-8}$ M) remained virtually unchanged by the 4E-T peptides (Table 1 and Fig. S4F-I). Altogether, these results suggest that 4E-T interactions with 4EHP enhance its binding to the m^7GTP cap structure.

DISCUSSION

Here, we describe a role for 4EHP in miRNA-mediated translation repression. Our results suggest that miRISC recruits 4EHP to target mRNAs through the CCR4-NOT complex. We propose that these interactions engender a closed-loop mRNP structure (Fig. 4), which resembles the cap-to-tail closed-loop mRNA conformation in translation initiation (41). A similar mechanism of translational inhibition had been described in *Drosophila* embryos wherein an interaction between d4EHP and Bicoid bridges the 5′ and 3′ ends of *caudal* mRNA (25). Thus, 4EHP-mediated mRNA looping appears as a general repressive mechanism implicated in various post-transcriptional regulatory pathways. This mechanism can also be employed by other RNA-binding proteins such as pumilio family members, tristetraprolin and nanos, which recruit CCR4-NOT to mRNAs (42).

An additional layer of complexity in understanding the exact mechanism of 4EHP action stems from the interaction of 4EHP with other protein partners. For instance, the GIGYF1/2 and 4E-T proteins bind to the same 4E-T binding motif on the 4EHP protein, and thus likely compete with 4E-T for this binding site. The GIGYF1/2-4EHP complex had been characterized as a translational repressor, notably as a cofactor of tristetraprolin (28, 29). Interestingly, GIGYF1/2 also associate with CCR4-NOT in both yeast and human cells (43, 44). Furthermore it was reported that GIGYF2 co-immunoprecipitates with AGO2, and tethering of GIGYF2 to a mRNA leads to its silencing (45). Therefore, it is conceivable that the miRISC/CCR4-NOT axis may recruit 4EHP via several parallel interactions, namely through interactions with both GIGYF1/2 and 4E-T.

Our model provides a tenable model of miRNA-mediated translation repression, but further investigation is necessary to fully resolve the interactions that occur at the cap of miRNA targets. An important conundrum is that the affinity of recombinant eIF4E for the cap is 30-100-fold greater than that of recombinant 4EHP. While binding to 4E-T increases 4EHP's affinity for the cap by ~4-fold, it remains much weaker than eIF4E (Fig. S4 and Table 1). The solution to this discrepancy may lie in additional interactions that prevail within the native miRISC effector complex and are missing from *in vitro* assays. Other interactions may further improve the affinity of 4EHP for the cap. Further study of the protein-protein interactions identified in our BioID survey may help resolve this conundrum. Alternatively, since the affinity of 4E-T for 4EHP is greater than that for eIF4E it is also possible that their interaction may enhance the proximal concentration of 4EHP near the cap to potentiate competition with eIF4E.

It was recently reported that 4E-T is recruited to mRNAs targeted by CCR4-NOT, and functions as an important co-factor of the mRNA decay machinery (13). This raises the intriguing possibility that 4E-T plays a dual role in miRNA-mediated silencing: 4E-T interactions with 4EHP potentiate translation repression, while its direct binding to eIF4E enables mRNA decay. Therefore, it would be interesting to determine the relative importance of eIF4E/4E-T versus 4EHP/4E-T contributions under different circumstances to miRNA action.

While significant progress had been made in understanding how they instigate mRNA deadenylation and decay, the mechanisms by which miRNAs repress translation remained unclear (1). Several recent studies demonstrated translational repression as an early step of miRNA-mediated silencing, which is followed by mRNA deadenylation and decay (4, 46, 47). Multiple studies now have shown that miRNAs interfere with translation initiation, specifically with cap recognition by eIF4E (3-5), and may induce the dissociation of eIF4E and eIF4G from target mRNAs (48). The model outlined here wherein 4E-T/4EHP interactions potentiate an interaction with the cap shines a new light on those prior findings.

Materials and Methods

BioID; Affinity purification (AP) and Trypsin digestion

For BioID experiments, stable cells were grown to ~75% confluency. Bait expression vectors and biotin were induced simultaneously (1 µg/ml tetracycline, 50 µM biotin). After 24 h of treatment, cells were rinsed once on the plate with ~20 ml PBS, then scraped into 1 ml of PBS. Cell pellets were collected by centrifugation (500xg for 5 min) and stored at -80°C for further processing. Cell pellets were thawed on ice and tared weight calculated. A 4:1 (v/w) ratio of ice-cold lysis buffer was added to the cells (50 mM Tris-HCl, pH 7.5, 150 mM NaCl, 1% NP40, 0.4% SDS, 1.5 mM $MgCl_2$, 1 mM EGTA, benzonase, Sigma protease inhibitors). Cells were dispersed with a P1000 pipette tip (~10-15 aspirations) and subjected to a rapid freeze/thaw cycle (dry ice to 37°C water bath). Lysates were rotated at 4°C for 30 min then centrifuged at 16,000xg for 20 min at 4°C. Supernatant was collected (with 20 µL aliquot saved for Western blot) into new tubes for affinity purification (AP). Samples were incubated with 20 µL (packed beads) of streptavidin-Sepharose (GE) (equilibrated in lysis buffer) with rotation overnight at 4°C. Beads were collected (500xg for 2 min), the supernatant discarded, and the beads transferred to new tubes in 500 µl of lysis buffer. Beads were washed once with SDS wash buffer (50 mM Tris-HCl, pH 7.5, 2% SDS), 2x with lysis buffer, and 3x with 50 mM ammonium bicarbonate, pH 8.0 (ABC) (all wash volumes = 500 µL with centrifugations at 500xg for 30 s). Beads were resuspended in 100 µl of ABC containing 1 µg of sequencing grade trypsin and gently mixed at 37°C for 4 h. 1 µg fresh trypsin was added and the samples were rotated overnight. Supernatant was collected (500xg for 2 min) and the beads washed with 100 µl of molecular biology grade H_2O and pooled with

peptides. Digestion was terminated by acidification with formic acid (50 µL of 10% stock = 2% final concentration). Samples were then centrifuged (16,000xg for 5 min) and ~90% of the sample was transferred to a new tube and dried with vacuum centrifugation.

Mass spectrometry (MS)

Dried peptides were resuspended in 10 µL of 2% formic acid, and 1.5 µL was analyzed by mass spectrometry (MS). Samples were injected by autosampler onto a spray tip formed from fused silica capillary column (0.75 µm ID, 350 µm OD) using a laser puller. The column had previously been loaded with 10-12 cm of C18 reversed-phase material (ZorbaxSB, 3.5 µm) by pressure bomb loading in MeOH and pre-equilibrated with buffer A. The column was placed in-line with a 5600 TripleTOF mass spectrometer (Sciex) equipped with a nanoelectrospray ion source connected in-line to a NanoLC-Ultra 2D plus HPLC system (Eksigent). Buffer A was 0.1% formic acid in water; buffer B was 0.1% formic acid in ACN. The HPLC gradient delivered an acetonitrile gradient over 120 min (2-35% buffer B over 85 min, 40-60% buffer B over 5 min, 60-90% buffer B over 5 min, hold buffer B at 90% 8 min, and return to 2% B at 105 min). The instrument was operated in the data-dependent acquisition (DDA) mode with 1 MS scan (250 ms; mass range 400-1250) followed by up to 20 MS/MS scans (50 ms each). Only candidate ions that were between 2-5 charge states were considered, and ions were dynamically excluded for 20 s with a 50 mDa window. The isolation width = 0.7, and minimum threshold = 200.

Luciferase assays

In experiments with miRNA reporters, U251, HeLa and MEFs were co-transfected in a 24-well plate with 20 ng of pGL3-*E2f* 3' UTR (37), pmiRGLO-3xmiR-19 (49) and pIS1-*Hmga2* 3'UTR (36), respectively. The pIS1 and pGL3 reporters were co-transfected with 5 ng of *Firefly* Luciferase (FL) and *Renilla* Luciferase (RL) plasmids, respectively. In tethering experiments, shCTR or sh4EHP HEK293T cells were transfected with 50 ng RL-5BoxB-A114-N40-HhR, 10 ng FL and 50 ng λN-fusion constructs per well in a 24-well plate using Lipofectamine 2000 (Thermo Scientific, 11668019) according to the manufacturer's instructions. For complementation experiments, 10 ng pcDNA5-3xFlag-4EHP (WT or Mut) were also added in these transfection mixtures. For 4EHP and 4E-T knockdown, $2x10^6$ cells were plated in a 10 mm culture dish and transfected with a final concentration of 25 nM of siRNA duplexes using Lipofectamine 2000 according to the manufacturer's instructions. After 24 h, cells were plated in a 24-well plate and transfected a second time with the plasmid mixture as described previously. Cells were lysed 24 h after transfection. Luciferase activities were measured with the Dual-Luciferase Reporter Assay System (Promega) in a GloMax 20/20 luminometer (Promega). RL activity was normalized to the activity of co-expressed FL and the normalized RL values are shown as repression fold relative to the indicated control.

Acknowledgments

We thank Devon Merkley, Pudchalaluck Panichnantakul, and Eliana Sacher for technical assistance; Maayan Shapiro, Mark A. Hancock, and Nadeem Siddiqui for discussions, and Chris Rouya, and Masahiro Morita for reagents. T. Yamamoto (OIST, Okinawa), N. Gehring (EMBL, Heidelberg) and Y. Tomari (IMCB, Tokyo) are gratefully acknowledged for their gifts of plasmids pME18S-flag-hCNOT1, pCI-λN-V5 and pAWH-RL-let7-A114-N40-HhR, respectively. The pGL3-*E2f*-3'UTR (WT and Mut) vectors were a gift from Joshua Mendell (Addgene plasmids 21170 and 21171). This work was supported by Canadian Institute of Health Research (CIHR) grants [MOP-7214 (to N.S.), MOP 123352 (T.F.D.)], and FDN 143301 (to A.-C.G.)], Terry Fox Research Institute grant TFF-122868 (to N.S.), and the National Science and Engineering Research Council (NSERC) grant RGPIN-2014-06434 (to A.-C.G.). T.F.D. is supported by the Fonds de la Recherche en Santé du Québec (FRQS), Chercheur-Boursier Senior Salary Award. S.M.J. is the recipient of a CIHR Postdoctoral fellowship. C.C. is supported by Fonds de Recherche du Québec – Santé (FRQS) and Fondation pour la Recherche Médicale (FRM) postdoctoral fellowships. E.M.C. is supported by Groupe de Recherche Axé sur la Structure des Protéines (GRASP). G.G.H. is supported by a Basic Research Fellowship from Parkinson Canada.

Author contributions

C.C. and S.M.J. designed research; C.C., S.M.J., E.M.C., and G.G.H. performed experiments; C.C., S.M.J., E.M.C., G.G.H., I.G., J.A., T.A., C.G.G., N.S.G., and A.C.G. analyzed data; M.R.F. provided critical feedback on the results and model; C.C. and S.M.J. wrote the manuscript; T.F.D. and N.S. provided general oversight, and edited the manuscript.

References

1. Jonas S & Izaurralde E (2015) Towards a molecular understanding of microRNA-mediated gene silencing. *Nat Rev Genet* 16(7):421-433.
2. Sonenberg N & Hinnebusch AG (2009) Regulation of translation initiation in eukaryotes: mechanisms and biological targets. *Cell* 136(4):731-745.
3. Pillai RS*, et al.* (2005) Inhibition of translational initiation by Let-7 MicroRNA in human cells. *Science* 309(5740):1573-1576.
4. Mathonnet G*, et al.* (2007) MicroRNA inhibition of translation initiation in vitro by targeting the cap-binding complex eIF4F. *Science* 317(5845):1764-1767.
5. Humphreys DT, Westman BJ, Martin DI, & Preiss T (2005) MicroRNAs control translation initiation by inhibiting eukaryotic initiation factor 4E/cap and poly(A) tail function. *Proc Natl Acad Sci U S A* 102(47):16961-16966.
6. Braun JE, Huntzinger E, Fauser M, & Izaurralde E (2011) GW182 proteins directly recruit cytoplasmic deadenylase complexes to miRNA targets. *Molecular cell* 44(1):120-133.
7. Chekulaeva M*, et al.* (2011) miRNA repression involves GW182-mediated recruitment of CCR4-NOT through conserved W-containing motifs. *Nat Struct Mol Biol* 18(11):1218-1226.
8. Fabian MR*, et al.* (2011) miRNA-mediated deadenylation is orchestrated by GW182 through two conserved motifs that interact with CCR4-NOT. *Nat Struct Mol Biol* 18(11):1211-1217.
9. Ozgur S*, et al.* (2015) Structure of a Human 4E-T/DDX6/CNOT1 Complex Reveals the Different Interplay of DDX6-Binding Proteins with the CCR4-NOT Complex. *Cell Rep* 13(4):703-711.
10. Waghray S, Williams C, Coon JJ, & Wickens M (2015) Xenopus CAF1 requires NOT1-mediated interaction with 4E-T to repress translation in vivo. *RNA* 21(7):1335-1345.
11. Kamenska A*, et al.* (2014) Human 4E-T represses translation of bound mRNAs and enhances microRNA-mediated silencing. *Nucleic Acids Res* 42(5):3298-3313.
12. Kamenska A*, et al.* (2016) The DDX6-4E-T interaction mediates translational repression and P-body assembly. *Nucleic Acids Res* 44(13):6318-6334.
13. Nishimura T*, et al.* (2015) The eIF4E-Binding Protein 4E-T Is a Component of the mRNA Decay Machinery that Bridges the 5' and 3' Termini of Target mRNAs. *Cell Rep* 11(9):1425-1436.

14. Chen Y*, et al.* (2014) A DDX6-CNOT1 complex and W-binding pockets in CNOT9 reveal direct links between miRNA target recognition and silencing. *Mol Cell* 54(5):737-750.
15. Mathys H*, et al.* (2014) Structural and biochemical insights to the role of the CCR4-NOT complex and DDX6 ATPase in microRNA repression. *Molecular cell* 54(5):751-765.
16. Rouya C*, et al.* (2014) Human DDX6 effects miRNA-mediated gene silencing via direct binding to CNOT1. *Rna* 20(9):1398-1409.
17. Dostie J, Ferraiuolo M, Pause A, Adam SA, & Sonenberg N (2000) A novel shuttling protein, 4E-T, mediates the nuclear import of the mRNA 5' cap-binding protein, eIF4E. *EMBO J* 19(12):3142-3156.
18. Joshi B, Cameron A, & Jagus R (2004) Characterization of mammalian eIF4E-family members. *Eur J Biochem* 271(11):2189-2203.
19. Rom E*, et al.* (1998) Cloning and characterization of 4EHP, a novel mammalian eIF4E-related cap-binding protein. *J Biol Chem* 273(21):13104-13109.
20. Wilhelm M*, et al.* (2014) Mass-spectrometry-based draft of the human proteome. *Nature* 509(7502):582-587.
21. Kubacka D*, et al.* (2013) Investigating the consequences of eIF4E2 (4EHP) interaction with 4E-transporter on its cellular distribution in HeLa cells. *PLoS One* 8(8):e72761.
22. Zuberek J*, et al.* (2007) Weak binding affinity of human 4EHP for mRNA cap analogs. *RNA* 13(5):691-697.
23. von Stechow L*, et al.* (2015) The E3 ubiquitin ligase ARIH1 protects against genotoxic stress by initiating a 4EHP-mediated mRNA translation arrest. *Mol Cell Biol* 35(7):1254-1268.
24. Okumura F, Zou W, & Zhang DE (2007) ISG15 modification of the eIF4E cognate 4EHP enhances cap structure-binding activity of 4EHP. *Genes Dev* 21(3):255-260.
25. Cho PF*, et al.* (2005) A new paradigm for translational control: inhibition via 5'-3' mRNA tethering by Bicoid and the eIF4E cognate 4EHP. *Cell* 121(3):411-423.
26. Cho PF*, et al.* (2006) Cap-dependent translational inhibition establishes two opposing morphogen gradients in Drosophila embryos. *Curr Biol* 16(20):2035-2041.
27. Villaescusa JC*, et al.* (2009) Cytoplasmic Prep1 interacts with 4EHP inhibiting Hoxb4 translation. *PLoS One* 4(4):e5213.
28. Morita M*, et al.* (2012) A novel 4EHP-GIGYF2 translational repressor complex is essential for mammalian development. *Mol Cell Biol* 32(17):3585-3593.
29. Fu R, Olsen MT, Webb K, Bennett EJ, & Lykke-Andersen J (2016) Recruitment of the 4EHP-GYF2 cap-binding complex to tetraproline motifs of tristetraprolin promotes repression and degradation of mRNAs with AU-rich elements. *Rna* 22(3):373-382.
30. Uniacke J*, et al.* (2012) An oxygen-regulated switch in the protein synthesis machinery. *Nature* 486(7401):126-129.
31. Roux KJ, Kim DI, Raida M, & Burke B (2012) A promiscuous biotin ligase fusion protein identifies proximal and interacting proteins in mammalian cells. *J Cell Biol* 196(6):801-810.
32. Teo G*, et al.* (2014) SAINTexpress: improvements and additional features in Significance Analysis of INTeractome software. *J Proteomics* 100:37-43.
33. Richter JD & Sonenberg N (2005) Regulation of cap-dependent translation by eIF4E inhibitory proteins. *Nature* 433(7025):477-480.
34. Marnef A & Standart N (2010) Pat1 proteins: a life in translation, translation repression and mRNA decay. *Biochem Soc Trans* 38(6):1602-1607.
35. Barisic-Jager E, Krecioch I, Hosiner S, Antic S, & Dorner S (2013) HPat a decapping activator interacting with the miRNA effector complex. *PLoS One* 8(8):e71860.

36. Mayr C, Hemann MT, & Bartel DP (2007) Disrupting the pairing between let-7 and Hmga2 enhances oncogenic transformation. *Science* 315(5818):1576-1579.
37. O'Donnell KA, Wentzel EA, Zeller KI, Dang CV, & Mendell JT (2005) c-Myc-regulated microRNAs modulate E2F1 expression. *Nature* 435(7043):839-843.
38. Baron-Benhamou J, Gehring NH, Kulozik AE, & Hentze MW (2004) Using the lambdaN peptide to tether proteins to RNAs. *Methods Mol Biol* 257:135-154.
39. Fukaya T & Tomari Y (2012) MicroRNAs mediate gene silencing via multiple different pathways in drosophila. *Molecular cell* 48(6):825-836.
40. Haghighat A & Sonenberg N (1997) eIF4G dramatically enhances the binding of eIF4E to the mRNA 5'-cap structure. *J Biol Chem* 272(35):21677-21680.
41. Kahvejian A, Roy G, & Sonenberg N (2001) The mRNA closed-loop model: the function of PABP and PABP-interacting proteins in mRNA translation. *Cold Spring Harb Symp Quant Biol* 66:293-300.
42. Chapat C & Corbo L (2014) Novel roles of the CCR4-NOT complex. *Wiley Interdiscip Rev RNA* 5(6):883-901.
43. Ash MR*, et al.* (2010) Conserved beta-hairpin recognition by the GYF domains of Smy2 and GIGYF2 in mRNA surveillance and vesicular transport complexes. *Structure* 18(8):944-954.
44. Ajiro M*, et al.* (2009) Involvement of RQCD1 overexpression, a novel cancer-testis antigen, in the Akt pathway in breast cancer cells. *Int J Oncol* 35(4):673-681.
45. Kryszke MH, Adjeriou B, Liang F, Chen H, & Dautry F (2016) Post-transcriptional gene silencing activity of human GIGYF2. *Biochem Biophys Res Commun* 475(3):289-294.
46. Bethune J, Artus-Revel CG, & Filipowicz W (2012) Kinetic analysis reveals successive steps leading to miRNA-mediated silencing in mammalian cells. *EMBO Rep* 13(8):716-723.
47. Djuranovic S, Nahvi A, & Green R (2012) miRNA-mediated gene silencing by translational repression followed by mRNA deadenylation and decay. *Science* 336(6078):237-240.
48. Zekri L, Kuzuoglu-Ozturk D, & Izaurralde E (2013) GW182 proteins cause PABP dissociation from silenced miRNA targets in the absence of deadenylation. *EMBO J* 32(7):1052-1065.
49. Mayya VK & Duchaine TF (2015) On the availability of microRNA-induced silencing complexes, saturation of microRNA-binding sites and stoichiometry. *Nucleic Acids Res* 43(15):7556-7565.
50. Reimand J*, et al.* (2016) g:Profiler-a web server for functional interpretation of gene lists (2016 update). *Nucleic Acids Res* 44(W1):W83-89.

Figure legends:

Table 1: Thermodynamic parameters for the interaction of eIF4E and 4EHP with m^7GTP in presence of 4E-T peptides, as determined by Isothermal Titration Calorimetry (ITC). See Fig. S4A for a schematic description of the peptides.

Fig. 1: Proteomic identification of the 4EHP and eIF4E proximal proteins. (*A*) High confidence protein interactions discovered by BioID for the indicated baits in HEK293 cells. CT (C-terminal) and NT (N-terminal) indicate the location of BirA* fusion protein in relation to the Bait protein. Average of two independent experiments for each tagged variant is presented. Interacting proteins were categorized according to their known functions. Avg-Spec shows the spectral counts for each indicated prey. BFDR: Bayesian False Discovery Rate. Complete list of the proximal proteins for each bait is presented in Dataset S1. (*B*) Gene ontology (GO) analysis of the BirA*-4EHP proximal proteins. Ten most significantly enriched biological processes identified using prohits-viz.lunenfeld.ca running g:Profiler (50) software are presented. Complete list of the enriched biological processes and molecular pathways is presented in Dataset S2. (*C*) HEK293T cells were transiently transfected with control or 3xFlag-4EHP plasmids. Two days later, cytoplasmic-cell lysate was immunoprecipitated using anti-Flag antibody in the presence of RNaseA. Western blot was performed using the specified antibodies. LE: long exposure; SE: short exposure. (*D*) Cytoplasmic-cell lysate from HEK293T cells was immunoprecipitated using anti-DDX6 or IgG antibodies. Western blot was performed using the specified antibodies. (*E*) HEK293T cells were transiently transfected with control or HA-PATL1 plasmid. Two days later, cytoplasmic-cell lysate was

immunoprecipitated using anti-HA antibody. Western blot was performed using the specified antibodies.

Fig. 2: 4EHP depletion impairs miRISC/CCR4-NOT-mediated translational silencing. (*A) Top*; Schematic representation of the RL-*Hmga2* 3´ UTR reporter. *Bottom;* WT and 4EHP-KO MEFs were co-transfected with RL-*Hmga2* 3´ UTR (WT) or (Mut), along with *Firefly* Luciferase. Luciferase activity was measured 24 h after transfection. *Renilla* values were normalized against *Firefly* levels, and repression fold was calculated for the RL-*Hmga2* 3´ UTR (WT) relative to RL-*Hmga2* 3´ UTR (Mut) level for each population. The same data are shown as relative RL/FL levels in Fig. S2B. (*B*) *Top*; Schematic representation of the FL-*E2f* 3´ UTR reporter. *Bottom;* Repression of FL-*E2f* 3´ UTR reporter in shCTR and sh4EHP U251 cells. U251 cells were co-transfected with pGL3-FL-*E2f* 3´ UTR (WT) or (Mut), along with *Renilla* Luciferase. Luciferase activity was measured 24 h after transfection. *Firefly* values were normalized against *Renilla* levels, and repression fold was calculated for the FL-*E2f* 3´ UTR (WT) relative to FL-*E2f* 3´ UTR (Mut) level for each population. **(***C*) Schematic diagram of full-length CNOT1 and the N-terminal, middle and C-terminal fragments used in 2D. The binding partners in CNOT1 are also depicted for each domain. (*D*) *Top*; Vectors expressing V5-CNOT1 and 3xFlag-4EHP (or control plasmid) were transfected into HEK293T cells. IP of V5-CNOT1 from RNaseA-treated extracts was performed using anti-V5 antibody. Purified proteins were analyzed by western blot with indicated antibodies. *Bottom*; HEK293T cells were transfected by vectors expressing V5-CNOT1 fragments (as described in 2C; N, N-terminal region (AA: 1-690); M, middle repressive module (AA: 1030-1600) and C, C-terminal region (AA: 1830-2376)) and 3xFlag-4EHP. Extracts were subjected to anti-

V5 IP, and the eluted fractions were analyzed by western blot with indicated antibodies. (*E*) 4EHP-mediates translational repression by tethered CNOT1 and GW182(SD). *Top;* Schematic representation of the RL-5*boxB*-A_{114}-N_{40}-HhR reporter. Control HEK293T cells (shCTR) or cells depleted of 4EHP (sh4EHP) were co-transfected with vectors expressing either λN-CNOT1, λN-GW182(SD) or λN control, along with RL-5*boxB*-A_{114}-N_{40}-HhR or RL-A_{114}-N_{40}-HhR, and *Firefly* Luciferase. RL luminescence was normalized against *Firefly* Luciferase level. Repression fold of RL-5*boxB*-A_{114}-N_{40}-HhR relative to RL-A_{114}-N_{40}-HhR expression is shown (*bottom*). Repression level of RL-5*boxB*-A_{114}-N_{40}-HhR by λN alone in shCTR cells was set as 1. (*F*) Rescue assay for λN-CNOT1-dependent silencing was performed, as described in E, in cells depleted of 4EHP. shCTR and sh4EHP HEK293T cells were transfected with the indicated plasmids in combination with constructs expressing shRNA-resistant versions of either 3xFlag-4EHP (WT), 3xFlag-4EHP^{W124A} cap-binding mutant (Mut) or empty vector (EV). The experiments illustrated in A, B, E and F are represented as mean values (± SD) of three independent experiments. The *P* value was determined by two-tailed Student's *t*-test: (ns) non-significant, (*) $P < 0.05$; (**) $P < 0.01$; (***) $P < 0.001$.

Fig. 3: 4EHP competes with eIF4E for binding to 4E-T. (*A*) HEK293T cells were transfected with vectors expressing HA-tagged WT 4E-T or the eIF4E/4EHP-binding mutant variants and 3xFlag-4EHP (or control vector). Lysates were immunoprecipitated using the anti-HA antibody. Western blot was performed using the specified antibodies. (*B*) HEK293T cells were transfected with vectors expressing HA-4E-T and increasing amount of 3xFlag-4EHP. Anti-HA IP and western blot were performed as described in A. (*C*) Binding assays with 4E-T/4EHP and 4E-T/eIF4E complexes. Constant amounts of

the HA-4E-T-bound beads were incubated with increasing concentrations of recombinant His-4EHP or His-eIF4E (0, 0.03, 0.06, 0.12, 0.25, 0.5 and 1 μM). After washing the beads, the retained complexes were eluted and analysed by western blotting with anti-His and anti-HA antibodies. (*D*) *Top*; For *in vitro* displacement assay, preassembled eIF4E–4E-T complexes bound on anti-HA agarose beads were incubated with increasing amounts of 4EHP (0, 0.11, 0.22, 0.44, 0.89, 1.78 μM). Proteins were eluted and analysed by western blot with the indicated antibodies. *Bottom*; Bar graph, obtained by densitometry analysis of western blot data, shows quantified intensities of eIF4E and 4EHP signals normalized against 4E-T. The data are expressed as mean values (± SD) of two independent experiments.

Fig. 4: Model of 4EHP-mediated translation repression by miRNAs. The recruitment of 4EHP to the miRNA target mRNA through the CCR4-NOT/DDX6/4E-T axis promotes its binding to the cap. The assembly of this complex is likely to initiate the formation of a closed loop structure (right panel) resembling the cap-to-tail closed-loop mRNA conformation involving eIF4G/PABP interaction (left panel).

Figure 1

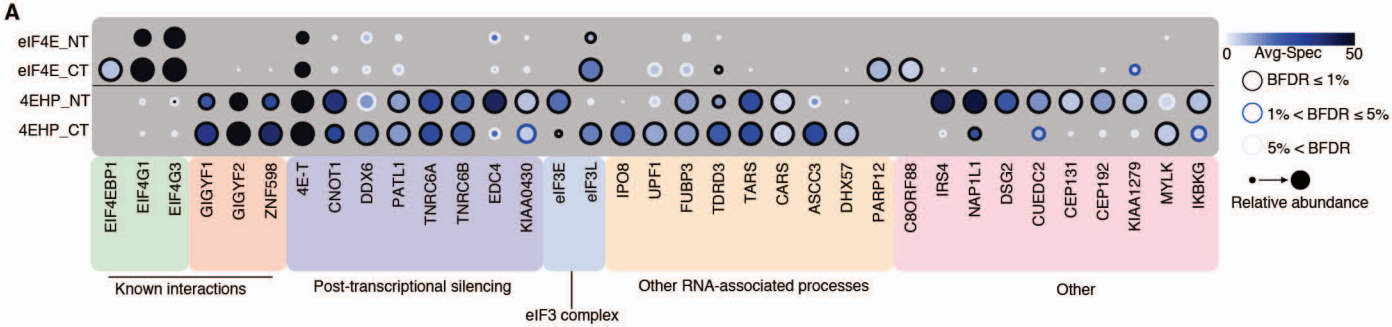
A
eIF4E_NT
eIF4E_CT
4EHP_NT
4EHP_CT
0
Avg-Spec
50
BFDR ≤ 1%
1% < BFDR ≤ 5%
5% < BFDR
Relative abundance
EIF4EBP1
EIF4G1
EIF4G3
GIGYF1
GIGYF2
ZNF598
4E-T
CNOT1
DDX6
PATL1
TNRC6A
TNRC6B
EDC4
KIAA0430
eIF3E
eIF3L
IPO8
UPF1
FUBP3
TDRD3
TARS
CARS
ASCC3
DHX57
PARP12
C8ORF88
IRS4
NAP1L1
DSG2
CUEDC2
CEP131
CEP192
KIAA1279
MYLK
IKBKG
Known interactions
Post-transcriptional silencing
eIF3 complex
Other RNA-associated processes
Other

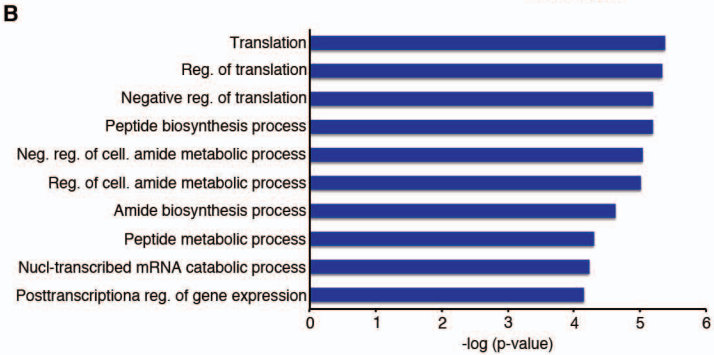
B
Translation
Reg. of translation
Negative reg. of translation
Peptide biosynthesis process
Neg. reg. of cell. amide metabolic process
Reg. of cell. amide metabolic process
Amide biosynthesis process
Peptide metabolic process
Nucl-transcribed mRNA catabolic process
Posttranscriptiona reg. of gene expression
0
1
2
3
4
5
6
-log (p-value)

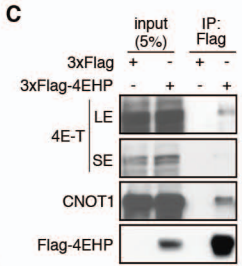
C
input (5%)
IP: Flag
3xFlag
3xFlag-4EHP
4E-T
LE
SE
CNOT1
Flag-4EHP

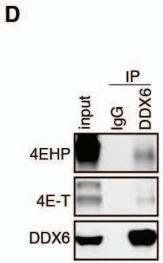
D
IP
input
IgG
DDX6
4EHP
4E-T
DDX6

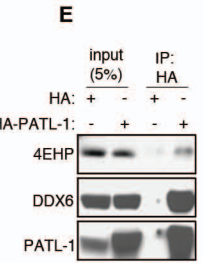
E
input (5%)
IP: HA
HA:
HA-PATL-1:
4EHP
DDX6
PATL-1

Figure 2

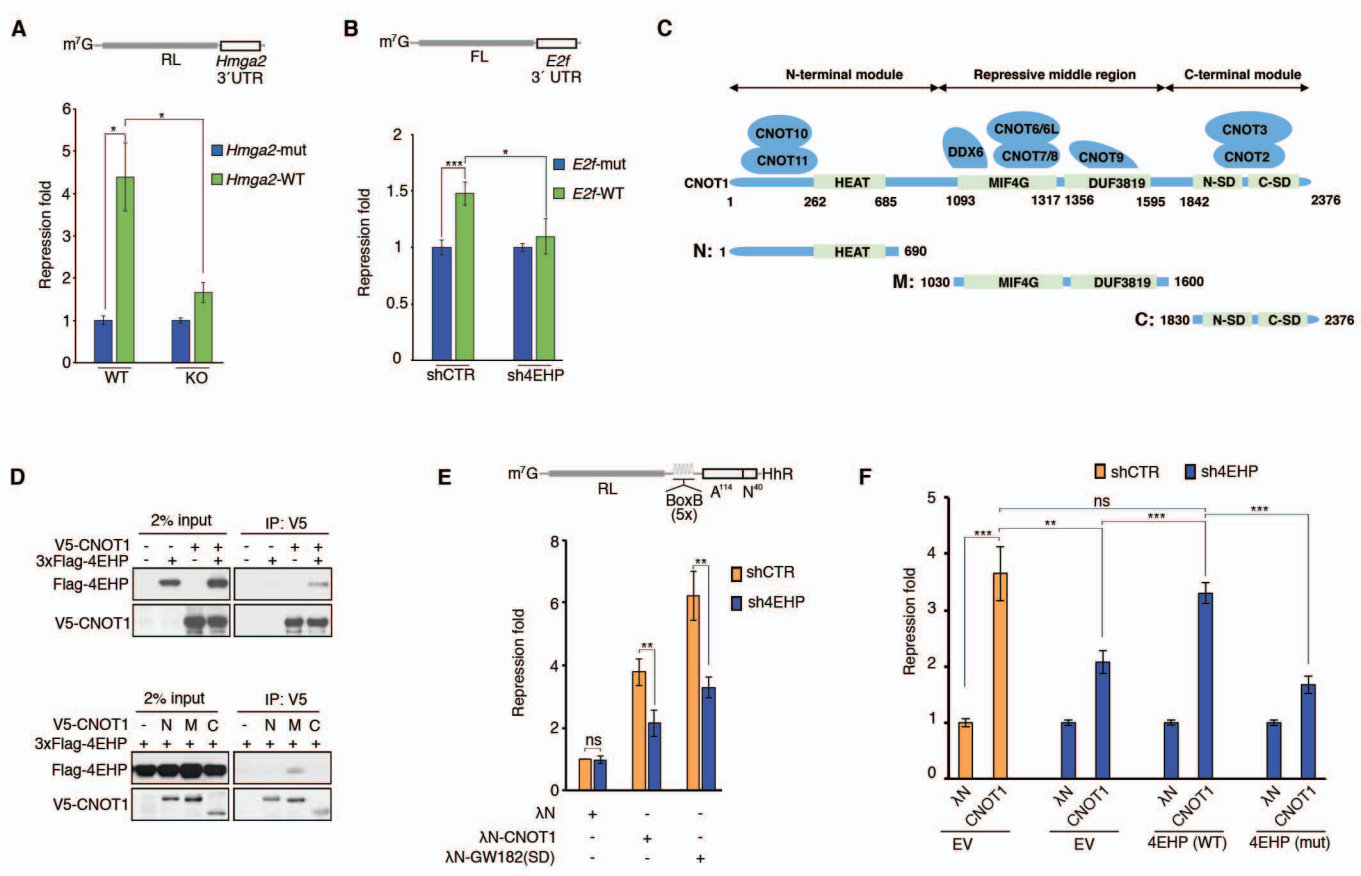
A
m7G
RL
Hmga2 3′UTR
Repression fold
Hmga2-mut
Hmga2-WT
WT
KO
B
m7G
FL
E2f 3′ UTR
Repression fold
E2f-mut
E2f-WT
shCTR
sh4EHP
C
N-terminal module
Repressive middle region
C-terminal module
CNOT10
CNOT11
DDX6
CNOT6/6L
CNOT7/8
CNOT9
CNOT3
CNOT2
CNOT1
HEAT
MIF4G
DUF3819
N-SD
C-SD
1
262
685
1093
1317
1356
1595
1842
2376
N: 1 HEAT 690
M: 1030 MIF4G DUF3819 1600
C: 1830 N-SD C-SD 2376
D
2% input
IP: V5
V5-CNOT1
3xFlag-4EHP
Flag-4EHP
V5-CNOT1
2% input
IP: V5
V5-CNOT1 - N M C
3xFlag-4EHP
Flag-4EHP
V5-CNOT1
E
m7G
RL
BoxB (5x)
A114
N40
HhR
Repression fold
shCTR
sh4EHP
ns
λN
λN-CNOT1
λN-GW182(SD)
F
shCTR
sh4EHP
Repression fold
ns
λN
CNOT1
EV
EV
4EHP (WT)
4EHP (mut)

Figure 3

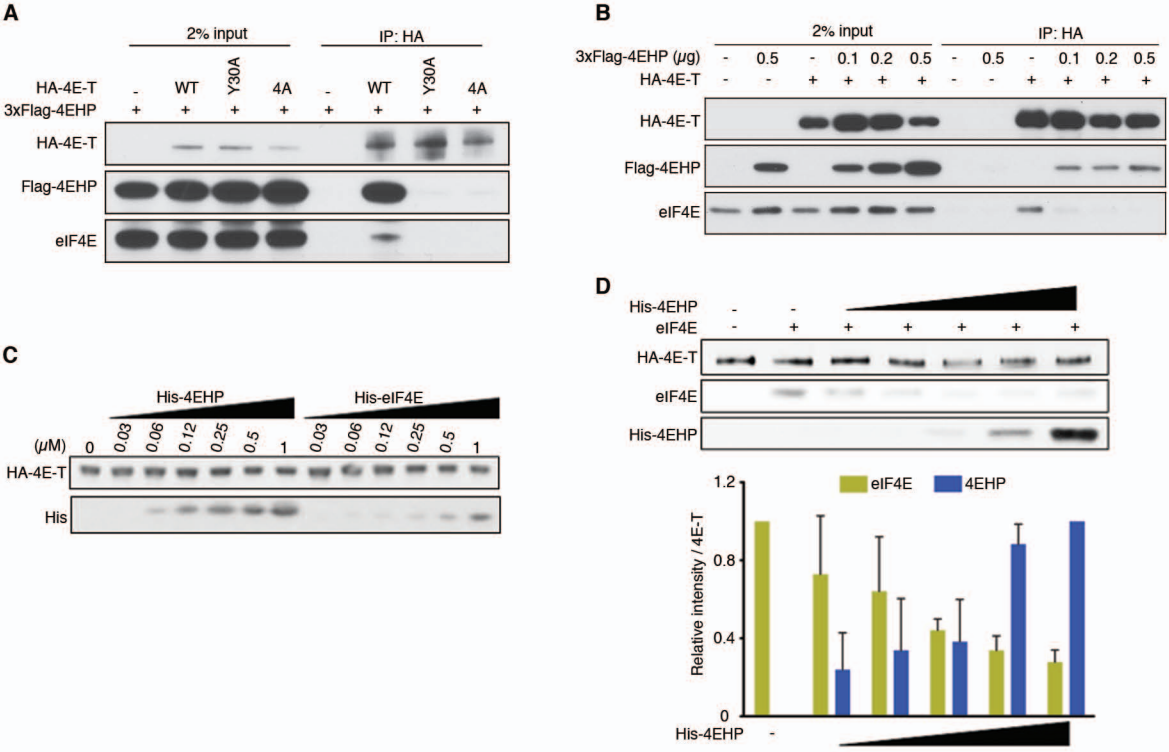
A
2% input
IP: HA
HA-4E-T
WT
Y30A
4A
3xFlag-4EHP
HA-4E-T
Flag-4EHP
eIF4E
B
2% input
IP: HA
3xFlag-4EHP (μg)
0.5
0.1
0.2
0.5
HA-4E-T
HA-4E-T
Flag-4EHP
eIF4E
C
His-4EHP
His-eIF4E
(μM)
0
0.03
0.06
0.12
0.25
0.5
1
HA-4E-T
His
D
His-4EHP
eIF4E
HA-4E-T
eIF4E
His-4EHP
eIF4E
4EHP
Relative intensity / 4E-T
1.2
0.8
0.4
0
His-4EHP

Figure 4

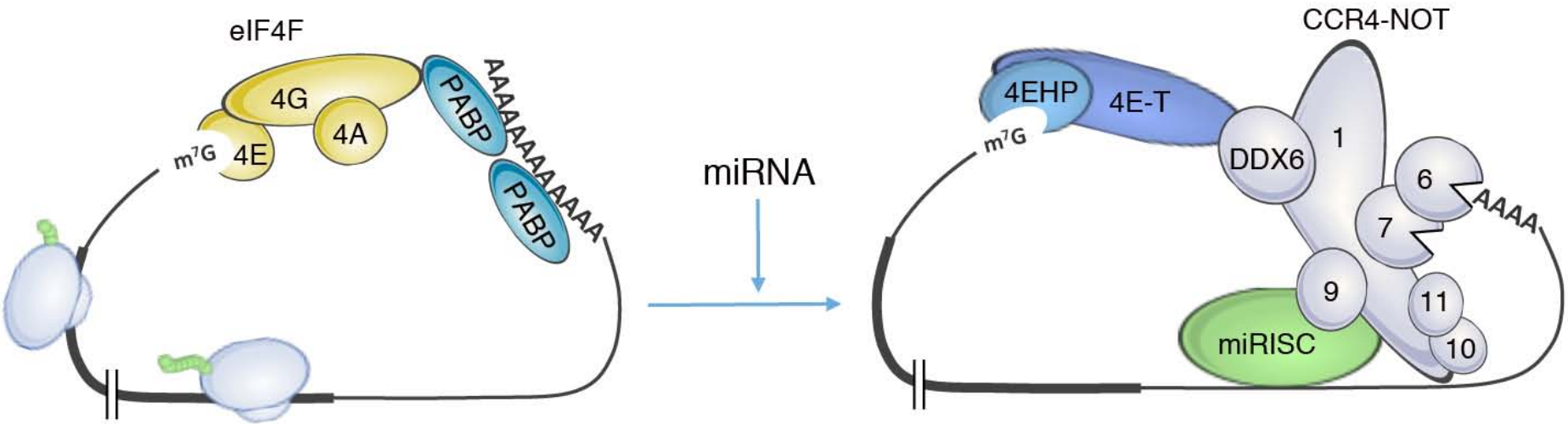
eIF4F
4G
4A
4E
m7G
PABP
PABP
AAAAAAAAAA
Active translation
miRNA
CCR4-NOT
4EHP
4E-T
m7G
DDX6
1
6
7
AAAA
9
11
10
miRISC
miRNA-mediated silencing

Figure S1

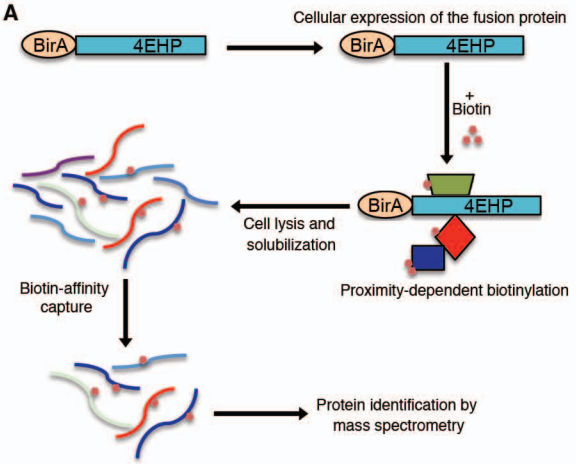
A
BirA
4EHP
Cellular expression of the fusion protein
BirA
4EHP
+
Biotin
BirA
4EHP
Proximity-dependent biotinylation
Cell lysis and
solubilization
Biotin-affinity
capture
Protein identification by
mass spectrometry

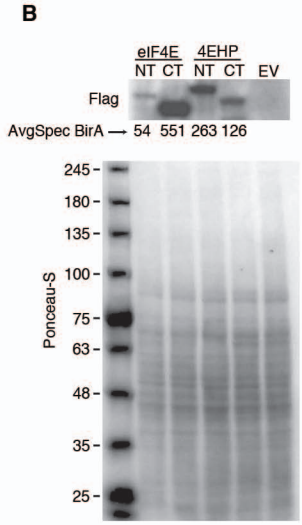
B
eIF4E
4EHP
NT CT NT CT EV
Flag
AvgSpec BirA → 54 551 263 126
245
180
135
100
75
63
48
35
25
Ponceau-S

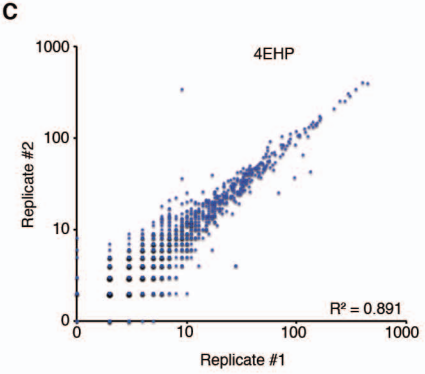
C
4EHP
1000
100
10
0
Replicate #2
0
10
100
1000
Replicate #1
R² = 0.891

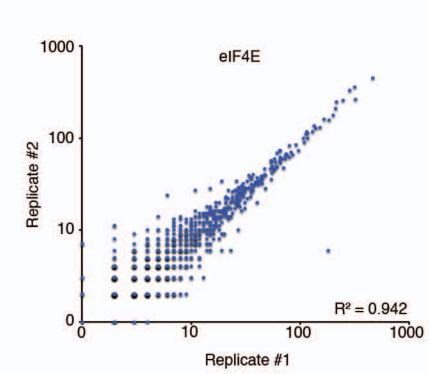
D
eIF4E
1000
100
10
0
Replicate #2
0
10
100
1000
Replicate #1
R² = 0.942

Figure S2

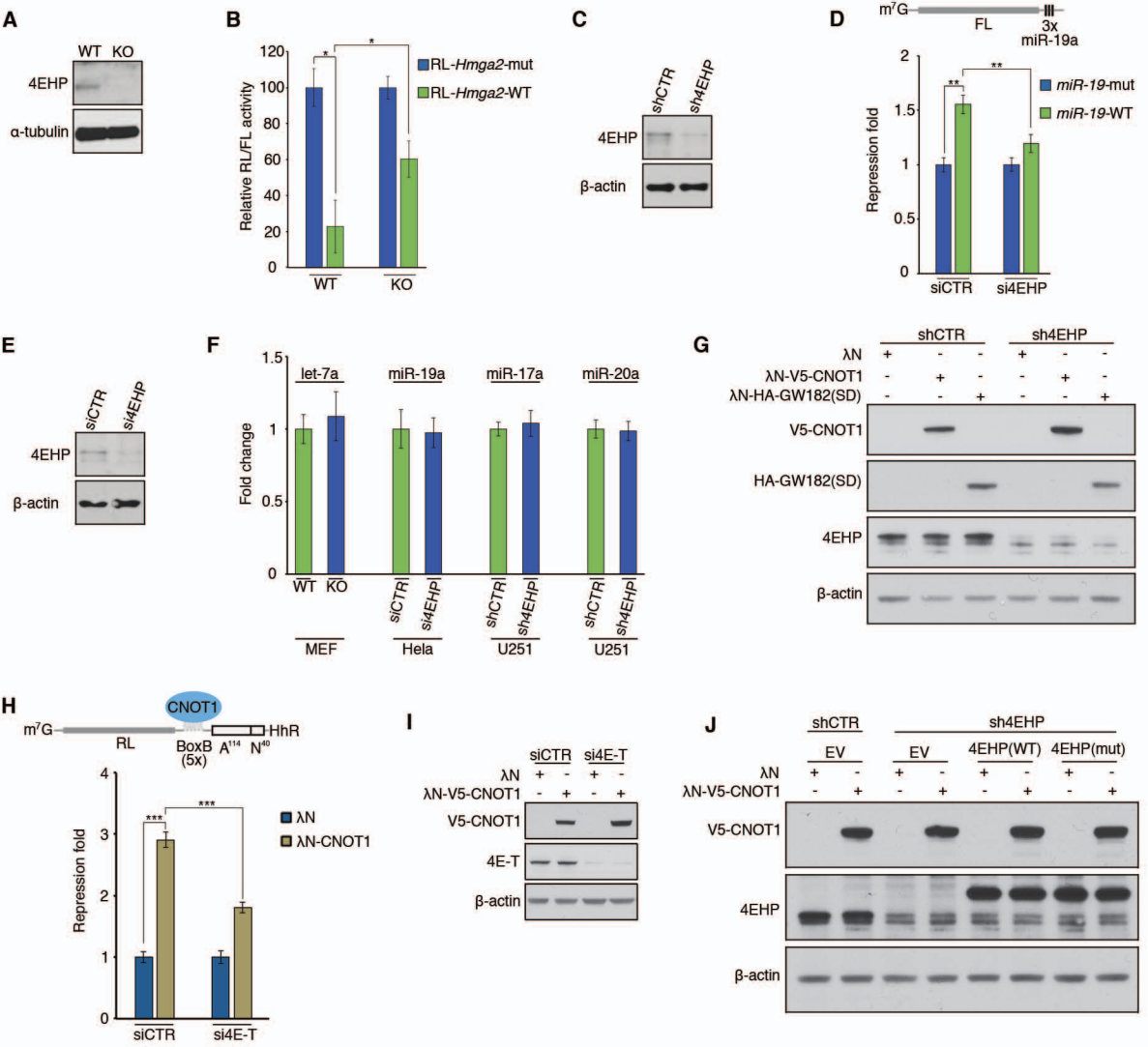
A
WT KO
4EHP
α-tubulin
B
Relative RL/FL activity
RL-Hmga2-mut
RL-Hmga2-WT
WT
KO
C
shCTR
sh4EHP
4EHP
β-actin
D
m7G
FL
3x miR-19a
Repression fold
miR-19-mut
miR-19-WT
siCTR
si4EHP
E
siCTR
si4EHP
4EHP
β-actin
F
Fold change
let-7a
miR-19a
miR-17a
miR-20a
WT
KO
siCTRl
si4EHPl
shCTRl
sh4EHPl
MEF
Hela
U251
U251
G
shCTR
sh4EHP
λN
λN-V5-CNOT1
λN-HA-GW182(SD)
V5-CNOT1
HA-GW182(SD)
4EHP
β-actin
H
CNOT1
m7G
RL
BoxB (5x)
A114
N40
HhR
Repression fold
λN
λN-CNOT1
siCTR
si4E-T
I
siCTR
si4E-T
λN
λN-V5-CNOT1
V5-CNOT1
4E-T
β-actin
J
shCTR
sh4EHP
EV
EV
4EHP(WT)
4EHP(mut)
λN
λN-V5-CNOT1
V5-CNOT1
4EHP
β-actin

Figure S3

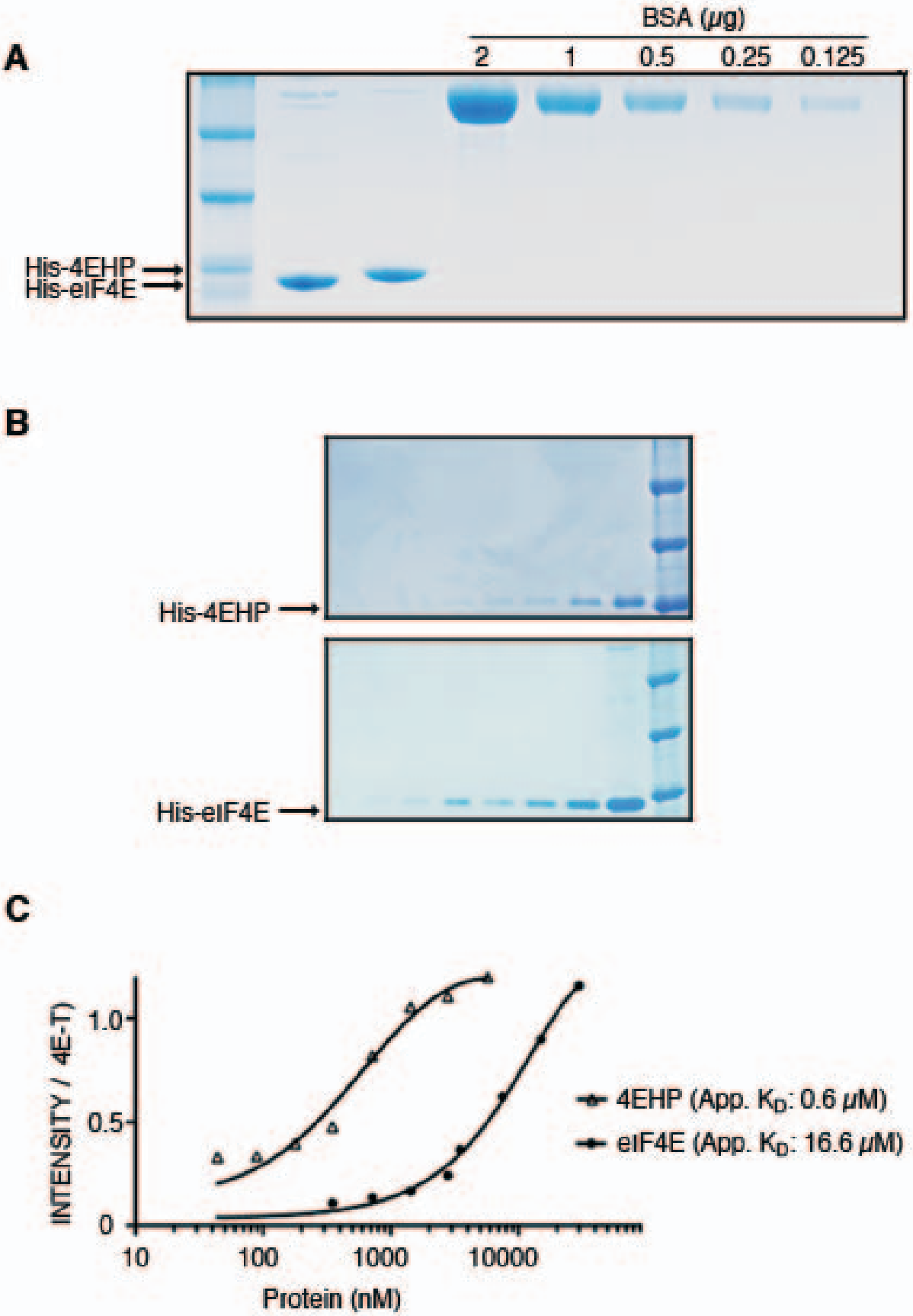
A
BSA (μg)
2
1
0.5
0.25
0.125
His-4EHP
His-eIF4E
B
His-4EHP
His-eIF4E
C
INTENSITY / 4E-T)
1.0
0.5
0
10
100
1000
10000
Protein (nM)
4EHP (App. K$_D$: 0.6 μM)
eIF4E (App. K$_D$: 16.6 μM)

Figure S4

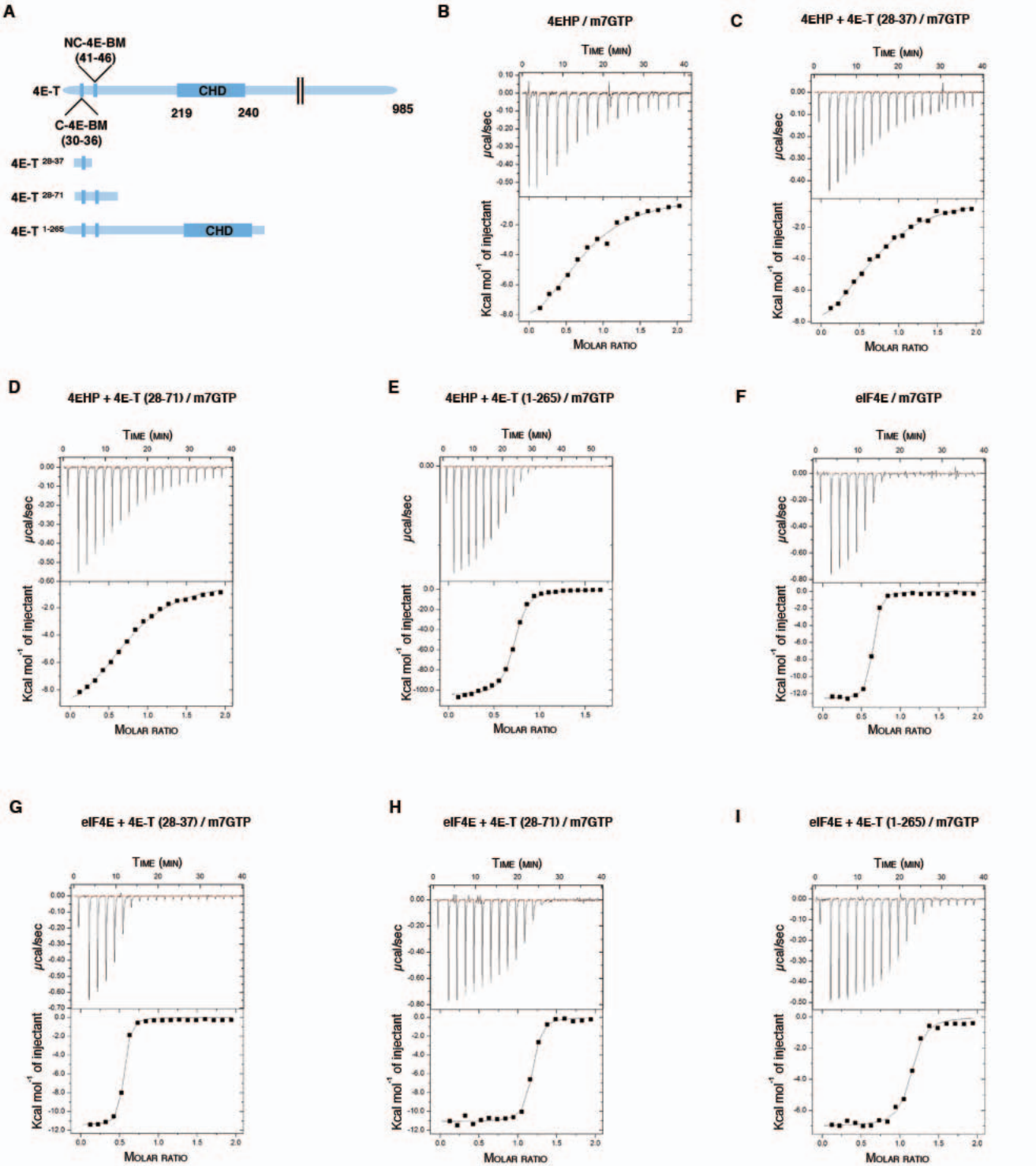
A
NC-4E-BM
(41-46)
4E-T
CHD
219
240
985
C-4E-BM
(30-36)
4E-T 28-37
4E-T 28-71
4E-T 1-265
CHD
B
4EHP / m7GTP
C
4EHP + 4E-T (28-37) / m7GTP
D
4EHP + 4E-T (28-71) / m7GTP
E
4EHP + 4E-T (1-265) / m7GTP
F
eIF4E / m7GTP
G
eIF4E + 4E-T (28-37) / m7GTP
H
eIF4E + 4E-T (28-71) / m7GTP
I
eIF4E + 4E-T (1-265) / m7GTP
Time (min)
µcal/sec
Kcal mol-1 of injectant
Molar ratio